

# Spectral Analysis of Experimental Ka-Band Propagation Measurements over the Australian LEO Microsatellite 'FedSat'

Thorsten Kostulski and Sam Reisenfeld

University of Technology, Sydney, Centre for Real-time Information Networks (CRIN)  
P.O. Box 123, Broadway NSW 2007, Australia  
{Thorsten.Kostulski, samr}@uts.edu.au

**Abstract.** The increased interest in the use of Ka band frequencies in satellite communications has prompted extensive propagation studies and the development of several rain fade models in the past, all of which are based on measurements from geostationary satellites only. Based on novel data, which has been experimentally obtained from the low earth orbit microsatellite 'FedSat', this paper addresses the spectral analysis of variable slant-path attenuation measurements under various weather conditions by examples, compares the results to similar GEO statistics and identifies potentially significant effects.

**Keywords:** Ka band, low earth orbit, satellite propagation, attenuation, spectral analysis, scintillation, rain fading.

## 1 Introduction

Motivated by bandwidth shortage in the classical satellite communication frequency bands (C, X, Ku), several experiments were undertaken to investigate the propagation conditions in the K/Ka band (18-36 GHz), predominantly in the years between 1974 and 1993 [1]. Signals at Ka band frequencies are severely affected by hydrometeors, e.g. rain and ice, and extensive empirical studies were conducted in order to model the statistics of signal attenuation and fade slopes. The data obtained from experimental, *geostationary* (GEO) satellites like ACTS, OLYMPUS and ITALSAT, in conjunction with the worldwide collection of precipitation data, has significantly contributed to the formation of widely used propagation models, such as the Crane model and various ITU Recommendations [2].

In recent years, low earth orbit (LEO) satellites and satellite constellations carrying Ka band payloads have increasingly emerged due to notable advantages in signal latency, launch cost, system capacity and earth station mobility. Since previously established propagation models were based on geostationary satellite measurements only, the demand has risen to adapt those models to LEO satellites. However, as a result of the dissimilar orbital characteristics, any measurements require the implementation of both spatial and frequency tracking in an earth station design. In contrast to the observation of significant rain events using ubiquitous GEO satellites,

the extremely reduced visibility of any one LEO satellite would have to coincide with any such event, making the successful data collection a very challenging undertaking.

The propagation measurement records of previous Ka band LEO satellite missions have been kept classified, commercial-in-confidence (Iridium, Teledesic) or sparsely published for unknown reasons (ROCSAT). The 2002 launch of the Australian LEO microsatellite 'FedSat' with a Ka band transponder payload represents the first and only mission with the goal of collecting and publishing Ka band propagation data from a LEO microsatellite [3]. Subsequent to the presentation and interpretation of attenuation phenomena in [4] and [5], this paper examines the fade slope and power spectral density statistics of received beacon and bent pipe mode signals under various weather conditions. It will be demonstrated that the knowledge of fade statistics is essential for the selection of the most suitable modulation scheme and therefore for optimum Ka band LEO satellite link design and performance.

## 2 Experimental Platform

### 2.1 Spacecraft and Earth Station

The research platform consists of the spacecraft and a fast-tracking earth station located in Sydney, Australia. Selected specifications of the satellite and its orbital properties are summarised in Table 1, most importantly the short orbital period and the very low transmit power. FedSat was designed and constructed almost entirely in Australia and carries various other experimental payloads besides the Ka band transponder.

**Table 1.** Selected orbital properties and Ka band payload specifications of FedSat

FedSat specifications		Ka band payload specifications	
Catalog No.	28598, 'FedSat'	Uplink frequency	29.93 GHz
Structure	50 cm cube, 58 kg	Downlink frequency	21.13 GHz
Inclination	98.5°	Transmit power	-6 dBW
Mean altitude	800 km	Antenna type	Multi-mode horns
Orbital period	100.85 min	U/L antenna gain	7.25 dB (max.)
Stabilisation	3-axis	D/L antenna gain	6.15 dB (max.)
Average power	35 W (per orbit)	Antenna beamwidth	120° isoflux approx.
Launch	14 Dec 2002 (Japan)	Receiver front end	Custom MMIC
Design lifetime	3 years	Operation modes	Beacon mode
Actual lifetime	4 years 10 months		Bent pipe mode

The corresponding earth station was designed for both Ka band data communication and propagation experiments. Budget restraints dictated the in-house design of the majority of the functional components, in particular the high-precision, electro-mechanical tracking system, the DSP-based, blind Doppler tracking subsystem and the entire real-time control and analysis software. Resulting from FedSat's near-polar LEO orbit, an X-over-Y tracking pedestal has been designed instead of a classical Az/El mount in order to overcome the keyhole problem. A functional block diagram of the earth station and a photo of the tracking pedestal are shown in Fig. 1.

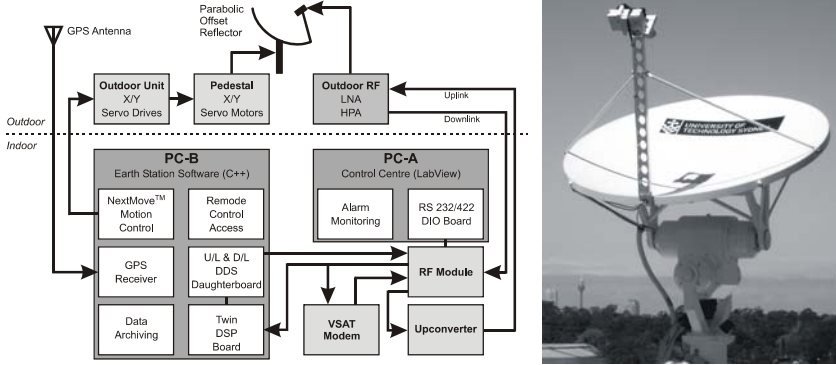


**Fig. 1.** Functional block diagram of the earth station (left), deployed outdoor unit (right)

In order to track the weak 20.13 GHz downlink signal transmitted by the rapidly moving spacecraft, the earth station design had to focus on accurate timing, high-precision spatial tracking, rapid signal acquisition and low-SNR frequency tracking. Due to the low downlink power budget, a dynamic tracking accuracy of  $0.1^\circ$  had to be maintained at all times, while using pointing angles pre-calculated from orbital elements. A novel, high-performance frequency estimation algorithm has been developed for the acquisition of the unknown carrier in noise and for subsequent Doppler shift compensation in the RF circuit [6]. The power level of the received signal was initially recorded at 70 ms intervals ( $f_s=14$  Hz), which was later enhanced to 6.7 ms intervals ( $f_s=150$  Hz) in order to capture rapid scintillations. For comparison, ‘high sampling rate’ measurements on ACTS were made at 20 Hz [7].

## 2.2 Pass Operation and Data Collection

Unlike preceding propagation experiments over GEO satellites, LEO satellite passes only allow the observation of a relatively short duration of around 15 minutes maximum. In the FedSat case, when elevation masking ( $30^\circ$  design limit) and low-elevation passes are taken into account, this interval is reduced to an average data record of only 5-10 minutes. Due to the earth rotation, the trajectory changes for each pass, and only very few theoretically visible passes higher than the required minimum elevation are actually long enough for data collection, as illustrated in Fig. 2. When operational restraints, such as the spacecraft power budget and resource sharing, are taken into account, the number of *practically* usable passes reduces to an average of 2 per week, or 7% of all visible passes. Compared to GEO experiments, this represents only 0.2% of the potential recording time. The presented statistics demonstrate that the chance of a pass occurring during significant events, like a rain storm, is exceedingly small, making the collection of meaningful data far more difficult for the LEO case. On the positive side, a trajectory from horizon to horizon means that it is possible to observe a variety of different weather conditions (rain, clouds, clear sky) during the same pass. For each experiment, the prevailing weather conditions along the trajectory and possible precipitation were recorded.

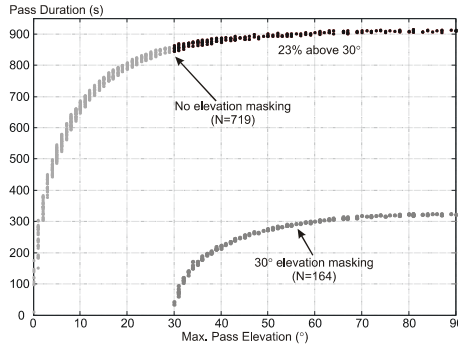


**Fig. 2.** Pass duration vs. maximum elevation statistics for all visible passes (top) and for passes with a  $30^\circ$  elevation mask (bottom) over a 200-day period

During the 30 months of earth station operation, 84 experiments have been conducted for various purposes. Usable propagation data was collected on 28 occasions and during various weather conditions. The majority of the recorded passes represent beacon mode reception, i.e. propagation effects on the 20.13 GHz downlink only. While this number of passes is too small for the proposal of an independent, empirical propagation model, several interesting attenuation, scintillation and low-angle fading phenomena have been observed (see Section 3).

The sampled propagation data is time-stamped, power-calibrated and processed on a 32-bit floating-point DSP. Subsequently, free-space path loss is subtracted, and additional attenuation introduced by the squint angle, i.e. the earth station receiver moving out of the satellite's footprint, is taken into account by modelling the spacecraft antenna gain pattern. In some cases, the signal was tracked less than  $6^\circ$  elevation on the descending path, which is below the design limit and therefore well outside the intended isoflux antenna footprint. In all cases, the accuracy of nadir pointing was confirmed through telemetry from FedSat's attitude control system.

### 3 Propagation Measurement Results

The collected data has been analysed in terms of atmospheric attenuation effects and power spectral density (PSD). In order to facilitate the understanding of LEO pass measurements, a time-domain example will be discussed first. Further charts can be found in [4] and [5].

#### 3.1 Time-Domain Analysis

Fig. 3 gives an example of a LEO pass recorded over 8 min 50 sec during inhomogeneous weather conditions, with a 6/8 stratus cloud cover on the ascending path, several isolated rain cells (approx. 5 mm/h) in the immediate vicinity and a light rain band on the descending path. The range varies between 872 km at maximum elevation ( $67^\circ$ ) and 2745 km at loss-of-signal (LOS). The small rain cells introduce a distinctive, localised rise in atmospheric attenuation of 5-6 dB, but do not appear to

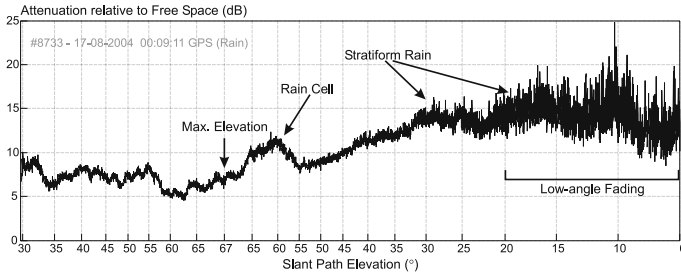


**Fig. 3.** Beacon signal attenuation recorded in the presence of scattered rain cells and stratiform rain, plotted in the time-domain versus the slant-path elevation angle,  $f_s=14$  Hz. The effects of localized rain attenuation and severe low-angle fading are clearly evident.

cause a significant increase in high-frequency fading. On the descending path, below  $30^\circ$ , the long slant path through the stratiform rain produces a significant rise in attenuation, and also an increase in scintillation of approximately 5 dB magnitude (low angle fading). Below  $10^\circ$  elevation, another interesting effect can be observed: Despite a longer path through the atmosphere, the measured average attenuation actually *decreases*, while very deep fades in excess of 10 dB occur. This is an indication of terrestrial multipathing, which limits the spectral efficiency of satellite links at very low elevation angles, and particularly on low link budgets.

### 3.2 Power Spectra Analysis

This section compares power spectral densities for data recorded during various weather conditions. While long-term statistics are readily available for GEO satellite experiments, the results presented in this section have been obtained from single LEO satellite passes with typically less than 10 minutes of data. In order to separate low-angle fading from other propagation effects, the data from each pass has been divided into two sets, *above* and *below* the  $30^\circ$  design limit. In the following figures, the dark trace represents samples recorded during high elevation, whereas the light trace corresponds to samples from below  $30^\circ$ . No windowing or interpolation has been applied, since this can lead to distortion. Three beacon mode examples at different weather conditions and one data set obtained from a bent pipe mode pass are shown.

**Beacon Mode Measurements.** In beacon mode, the Ka band transponder transmits a continuous carrier signal on 20.13 GHz. Meteorological data, including publicly available precipitation information and rain radar images, are recorded along with the pass information.

*Clear Sky Conditions.* The PSD in Fig. 4 was calculated from a pass on a clear, low-humidity day over 9 min 30 sec. An approximate frequency asymptote is also indicated. The graph shows the familiar decay of the spectral components with a first-order characteristic. The fairly similar high-frequency power levels of both high-angle and low-angle samples lead to the conclusion that not much turbulence was present in the atmosphere during the pass. There is no evidence of low-angle fading effects.

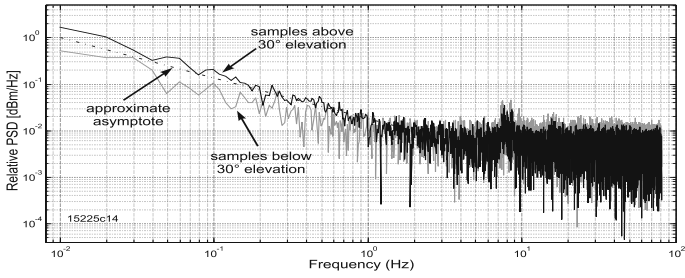


**Fig. 4.** PSD of a typical clear sky pass (max. elevation 83°, LOS at 14°,  $f_s=150$  Hz)

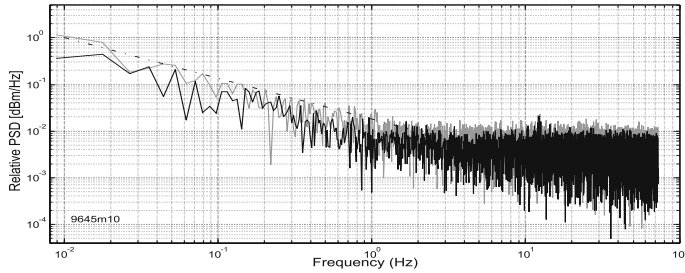


**Fig. 5.** PSD of a pass with 8/8 stratus cloud cover (max. elevation 61°, LOS at 10°,  $f_s=150$  Hz)

*Cloudy Conditions.* Fig. 5 shows the PSD representation of a LEO pass during overcast conditions with a thick stratus cloud cover, but no precipitation. The characteristics, such as 1<sup>st</sup> order behaviour and low/high angle power levels, are similar to the clear sky case, however scintillations are slightly higher around 1 Hz.

*Rain Cells.* The example in Fig. 6 represents the PSD of the same pass as in Section 3.1 (Fig. 3). Despite the lower sampling rate, the comparison between the high and the low-angle PSD leads to interesting observations. Both PSDs exhibit the same asymptotic slope as in the other cases, however there is no distinct corner frequency for the high-elevation section. The low-angle PSD segment appears to level out one order of magnitude earlier than without precipitation, which is a clear indication of rain fade occurring along a very long effective path. In addition, the

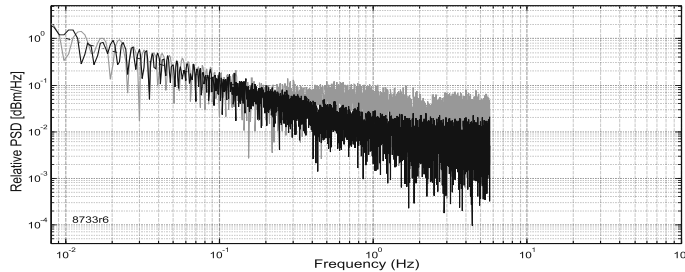


**Fig. 6.** PSD of the rain-affected beacon pass from Fig. 3 (max. el. 67°, LOS at 6°,  $f_s=14$  Hz)

power level of high-frequency components is considerably elevated, which means that high-frequency scintillations introduced by rain at low elevation angles are very significant. This observation has far-reaching implications on the optimum utilisation of the channel capacity, as discussed in [8].

**Bent Pipe Mode Measurements.** The traces in Fig. 7 have been derived from a bent pipe mode pass during overcast conditions. In this operation mode, a Doppler pre-corrected uplink carrier signal is transmitted by the earth station and therefore received by the LEO satellite at a fixed frequency of 29.93 GHz. On the uplink, the signal is already affected by tropospheric attenuation and fading. After frequency conversion and amplification by the Ka band transponder, it is re-transmitted on the 20.13 GHz downlink, where it is subjected to more channel attenuation and fading.

The plot illustrates the *composite* effect of uplink and downlink attenuation. Both PDSs tend to follow the same asymptotic slope and power level (at higher frequencies) as in the beacon mode example, however the ‘corner’ is less pronounced.

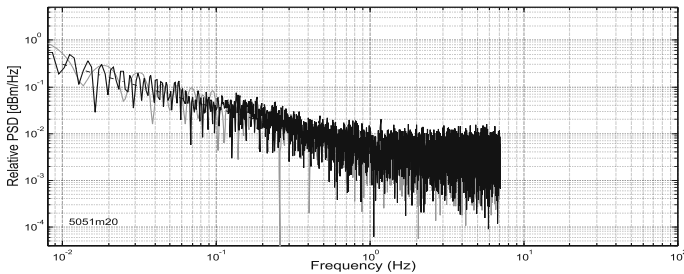


**Fig. 7.** PSD of a bent pipe mode experiment (max. el.  $62^\circ$ , LOS at  $20^\circ$ ,  $f_s=14$  Hz)

## 4 Validation of Results

### 4.1 Comparison with PSD Results from GEO Satellite Experiments

Since the results introduced in this paper are amongst the first in the field of LEO Ka band propagation, validation *in principle* is sought from the very well published area of Ka band propagation over GEO satellites. Due to the nature of LEO passes, the observation time was restricted to several minutes only, limiting the analysis of low-frequency components to those above 0.01 Hz.

When comparing LEO with GEO data and models [9], it is important to recall that all samples were recorded during *rapid* movement of the satellite across the sky, which implies a superposition of signal fluctuations due to spacecraft motion and of tropospheric effects, such as absorption and scattering by hydrometeors in a turbulent channel. Figs. 17 and 18 in [7] show two PSD charts obtained from a Ka band beacon on a GEO satellite (ACTS) at two separate locations, sampled at 20 Hz. At Norman, Oklahoma (OK), the fixed elevation angle was  $49.1^\circ$ , and at Fairbanks, Alaska (AK), the fixed elevation angle was  $7.9^\circ$ . The observation period of each event is comparable to the duration of a typical LEO pass. The authors state that the PSDs are consistent with theoretical predictions of clear sky, cloudy and light rain conditions.

For atmospheric conditions without heavy precipitation, both LEO and GEO results follow a similar curve shape (asymptote, 1<sup>st</sup> order characteristic). At higher elevation angles (OK), the ‘corner frequency’ lies at about 0.6 Hz, whereas for a longer path through the atmosphere (AK), it moves above 1 Hz with a less pronounced ‘corner’. The latter observation is consistent with the results presented in this paper. The slightly rounder decay exhibited in *bent pipe mode* can be explained by Fig. 17 in [7], in which the 27 GHz PSD rolls off slightly slower than the 20 GHz PSD. These comparisons with GEO data suggest a general validity of the results, however some effects, especially the significantly raised, high-frequency power levels at low elevation angles during rain require further investigation in a LEO context.

## 5 Conclusion

The successful collection of scarce Ka band data from the LEO microsatellite ‘FedSat’ provides a new opportunity for the investigation of propagation effects. This paper has presented several power spectral density graphs of received beacon and bent pipe mode signals under various weather conditions. In some cases, the measured data suggests that LEO scintillations have a wider bandwidth than previously observed on GEO satellites, which is a potentially important finding and may be significant for the design of multi-level modulation schemes and for the selection of sustainable data rates on future Ka band LEO satellite links. Forthcoming work will include the investigation of fade slope distributions and the statistical modelling of the observed effects.

## References

1. Chakraborty, D., Davarian, F., Stutzman, W.L.: The Ka-Band Propagation Measurement Campaign at JPL. *IEEE Ant. and Prop. Magazine* 35(1), 7–12 (1993)
2. Crane, R.K., Dissanayake, A.W.: ACTS Propagation Experiment: Attenuation Distribution Observations and Prediction Model Comparison. *IEEE Proc.* 85(6), 879–892 (1997)
3. Kostulski, T., Reisenfeld, S.: Ka band Propagation Experiments on the Australian Low-Earth Orbit Microsatellite ‘FedSat’. In: 6th Australian Communication Theory Workshop, Brisbane, Qld, pp. 95–99 (2005)
4. Kostulski, T., Reisenfeld, S.: Variable Slant-Path Ka-Band Propagation Measurements on the Australian LEO Microsatellite ‘FedSat’. In: 11<sup>th</sup> Ka and Broadband Communications Conference, Rome, pp. 365–372 (2005)
5. Kostulski, T.: Ka Band Propagation Experiments on the Australian Low Earth Orbit Microsatellite ‘FedSat’, PhD Thesis (Engineering), Univ. of Technology, Sydney (2008)
6. Reisenfeld, S.: A Highly Accurate Algorithm for the Estimation of the Frequency of a Complex Exponential in Additive Gaussian Noise. In: 5<sup>th</sup> Australian Communications Theory Workshop, Newcastle, NSW, pp. 154–158 (2004)
7. Mayer, C.E., Jaeger, B.E., Crane, R.K., Wang, X.: Ka-Band Scintillations: Measurements and Model Predictions. *IEEE Proc.* 85(6), 936–945 (1997)
8. Miodrag, F., Vilar, E.: Optimum Utilization of the Channel Capacity of a Satellite Link in the Presence of Amplitude Scintillations and Rain Attenuation. *IEEE Trans. Comm.* 38(11), 1958–1965 (1990)
9. Gremont, B.C., Miodrag, F.: Spatio-Temporal Rain Attenuation Model for Application to Fade Mitigation Techniques. *IEEE Trans. Ant. Prop.* 52(5), 1245–1256 (2004)